Surface Roughness Prediction of Thin-Walled Parts Impacted by Radial Depth of Cut Variations During Peripheral Milling Process

Abainia Sadredine

Division Productique Robotique,
Centre de Développement desTechnologies Avancées (CDTA), Algiers
Algeria

During the peripheral milling process, great transverse displacement vibrations of the thin-walled part are occurred under the acting of milling tool edge forcesdue to their low dynamic rigidity and the radial depth of cut ae variations. In this work, the main surface roughness parameters are evaluated for stable milling process conditions through maximum radial displacements determined by a theoretical method and a finite element (FE) computation utilizing numerical simulations. The cutting tooth edge forces are calculated along the effective part for each tooth tool engaged into part material in discrete spatial and time steps using flat-end mills. Finally, the radial displacements are confronted, which are close in magnitude and in profile shape trend. Therefore, the generated cutting tooth edge forces showed gradual stabilities while changing the parameter ae from 05 mm to 0.75 mm, respectively. Then, the parameters R_a and R_q contribute more to these stabilities than R_v.

Keywords: *Thin-walled part, cutting force tooth edge, radial depth of cut fluctuation, finite element, surface roughness parameter*

1. INTRODUCTION

In the aerospace industry, thin-walled workpiece milling is a critical task, and the machining vibration is a major issue for the accuracy of the final part [1]. Then, workpiece dynamics is the dominant factor that should be considered in chatter prediction of peripheral milling of thin-walled parts. In an ideal peripheral milling process, the machined surface can be seen as a reflection of relative movement between the tool and the workpiece. Due to the cutting edge's spiral form, the tool teeth' cycloidal path varies along the different axial depths [2]. Further, the workpiece vibrations cause unacceptable waviness and chatter marks on the part surfaces, thus producing defective parts [3-4]. For this, many researchers focused on the modeling of peripheral milling surface topography considering vibrations that are closely related to the milling force [2] and the deformation prediction using numerical simulation based on the finite element (FE) method [5]. Then, optimizing the machining conditions for this type of milling requires the determination of a suitable radial cutting depth of cut *ae* to minimize in deep the dynamical behavior of milling cutting, which is not yet achieved and remains deficient, according to the workpiece displacement vibrations. From the related research existing in the technical literature and among these researches, as in the work of Yue et al. [6] where they established a coupling relationship between a milling force model and the bending elastic deformation of thin-walled parts to predict their surface errors generated by discretized micro-element cutting edges for a single flute cutting. They found that the entry tool angle and the instantaneous micro-element thickness are mainly affected by the dynamic deformation of the part. Using shell theory, Fei et al. [7] computed the dynamic cantilever plate deformation along the milling path. The dynamic deformation governing the equation to the thin part is resolved in the high-frequency part excited by measured milling forces. Shi et al. [8] investigated the dynamic response of a cantilevered thin-walled rectangular plate under the influence of the variable thickness and cutter moving path. The governing equation of motion of the flexible workpiece in transverse vibration is resolved by the Rayleigh-Ritz method to calculate the transverse displacements, which are verified with those obtained by the finite element method (FEM). Fei et al. [9] proposed an analytical dynamic deformation of thin-walled parts based on the thin plate theory in side milling, taking the measured milling force as moving excitation. Subsequently, the analytical results show better accuracy and less cost time than FEM results. Zhang et al. [10] searched the influence of the time variation of deflection and dynamic characteristics of the thin-walled workpiece during flank milling to show the chatter domains in different process positions. Bolar et al. [11] simulated the milling of thin-wall components using FEM simulations. They noted that maximum deflections occurred at the free end of the wall compared to its center and base. Khandagale et al. [12] presented a developed mathematical model which gives the time response of a thin rectangular cantilever plate under moving milling forces. Hence, the authors concluded

Received: Septembre 2022, Accepted: April 2023
Correspondence to: Dr Abainia Sadredine
Division Productique Robotique,
CDTA-Algiers, Algeria
E-mail: s_abainia@yahoo.fr
Doi: 10.5937/fme2303284S

that the model's effectiveness is useful in high-speed machining with a higher depth of cut for thin impeller blades. Masmali et al. [13] proposed a dynamic analytical modeling approach for predicting the displacements for thin-walled workpieces. They concluded that the feedback of the displacement amplitude was linked to a cutting force model. Then, they concluded that the influence of the dynamic displacement of the workpiece is related to the acting chip load. Chen et al. [14] established a predicting machining deformation model by considering a multilayer active compensation method when machining a thin-walled part with single-tooth end milling to improve the machining accuracy. Hence, the compensation per layer makes smaller machining errors, and the errors are more uniform. Globocki et al.[15] searched the influence of the optimal machining strategy and the optimal machining parameters on the machining time, surface roughness, and part shape accuracy when milling parts with some geometries. They concluded that their effects were significant. Zeng et al. [16] proposed a dynamic model of the workpiece-fixture-cutter system and a fixture design method for predicting the vibration displacement responses with the aim of suppressing the machining vibration of the flexible workpiece originating from the cutting forces. Afterward, it is concluded that the vibration characteristics of the workpiece-fixture system are improved and can effectively suppress the machining vibration to enhance the precision of the final part.

From the previously explored works above, some deficiencies can be drawn as in the following, where the whole tool geometry should be taken for results validation. Further, integrating the rigidity influence in deep is useful. In addition, there is no standard design workpiece-fixture-cutting tool system to attenuate the machining vibration for this type of milling.

Comparing our work according to some research explained above, a difference appears regarding the analytical displacement response prediction for peripheral milling, where the proposed approach is based on the beam theory rather than thin plate theory and shell theory. Further, the integral of Duhamel is utilized as a solution for their adequation to a random cutting force.

For this, the basic motive of this research is to evaluate the impact of the radial depth of cut *ae* variations on the generated cutting tooth edge forces. Then, for some successive milling passes, surface roughness deviations left by the previous cutting tooth are determined based on the maximum displacement calculations for certain surface roughness parameters.

In the present work, the peripheral milling surface roughness parameters are calculated based on the maximum displacement of the cantilevered thin-walled part in bending vibrations under acting the radial cutting forces along scheduled tool path positions by proposing a mathematical formulation and finite element simulations method. Based on the mechanical cutting force modeling, the cutting edge forces are calculated along a straight tool path, taking into account the geometric parameters of the used flat-end milling tool, the combination of milling cutting tool and workpiece material, the machining conditions, especially the parameter *ae* which considered as a variable. Afterward, the effect of regenerative of the machined surface is integrated by adjusting the parameter, ae which has been linked to surface roughness values to control generated cutting forces at each tooth passing period for some machining passes in simulations. Finally, comparisons between the obtained types of results are performed for verifications and evaluations.

In brief, the global approach is shown in the following flowchart in Figure 1.

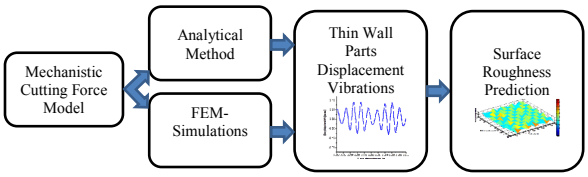

Figure 1. Flowchart of the global approach.

2. MODELLING OF THE FLEXIBLE THIN-WALLED PART

During the milling process of the thin-walled part, great displacements occur in the radial y-direction due to low rigidity compared to its high stiffness level in x and z directions. In addition, little contributions to the dynamic deformation of the thin-walled workpiece cutting forces along the directions of x and z are neglected. Afterward, also due to the typical thinner part with fixture constraint, which is used in the aerospace industry, then it is approached as a rectangular cantilever beam, as shown in Figure 2. Then, the transverse displacement vibrations of the thin-walled workpiece in the y-direction are considered under the acting of the cutting tool edge forces. However, consequently, the surface roughness should be predicted. Afterward, the main assumptions during modeling are the following:

- The workpiece is considered to be flexible compared to the cutting tool, which is assumed to be rigid,
- The influence of the material removal during the peripheral milling process is neglected, and their effect on the dynamic characteristics of the workpiece is also neglected,
- The thin-walled workpiece milling process moves along the z-direction only (Fig. 2), normal to the machined wall surface schematized with a single degree of freedom model vibrations in the y-direction (Fig. 3).

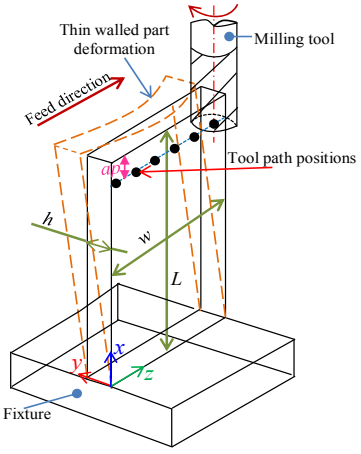

Figure 2. Thin-walled part deformation.

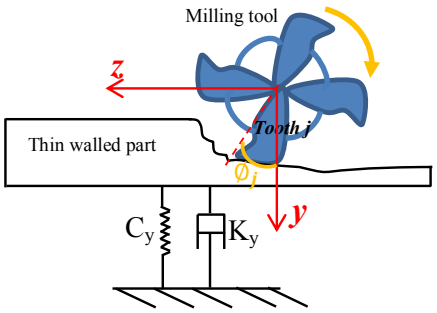

Figure 3. Model of thin-walled part vibrations in the y-direction.

As shown in Figure 2 and for more description, if considering the workpiece as a rigid body, in this case, it is presented with solid lines, and the radial depth of cut *ae* is theoretically maintained fixed. While in the opposite case, the workpiece is assumed to be a flexible body sketched with dotted lines, and the parameter *ae* becomes variable. Furthermore, in the y-direction, the displacement of the thin-walled part generates fluctu–ations by increasing and decreasing *ae* as in Figure 3, which further affects the milling force [17]. Therefore, when the machining system is stable, there is a certain relationship between the milling force, the parameter *ae*, and the displacement response caused by the vibration of the workpiece [17]. From this viewpoint, the para–meter *ae* is taken as an influence variable in this study. For this reason, the surface roughness prediction model of the thin-walled part is combined with the mechanical cutting force to estimate the main machined surface roughness parameters from their maximum displace–ments, which are occurred at the top area of the canti–levered thin-walled part, where it is the aim from this study.

2.1 Surface roughness description

The machined surface in the milling process is generated by each cutting edge composed of the tool geometry acting on the thin-walled workpiece and generates gradual dynamic displacements, which vary according to the milling tool path position and the elementary cutting edge of the discretized tool. Then, evaluating its main surface amplitude parameters in the engineering practice is depicted in Figure 4.

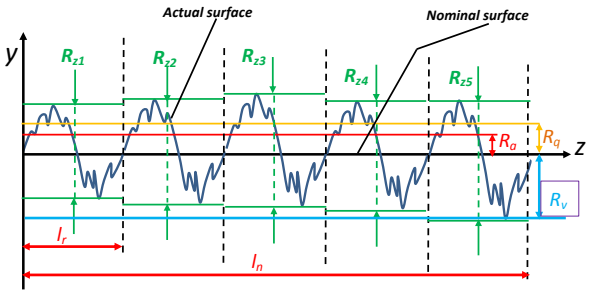

Figure 4. Considered main roughness parameters.

With: R_a: Arithmetic average roughness
R_q: Root mean square of the surface roughness
R_v: Maximum profile valley depth
R_{zi}: Average maximum peak to valley of five conse–cutive sampling lengths within the measuring length.
l_n: Evaluation length
l_r: Sampling length

3. MILLING CUTTING FORCE MODELLING

In the milling process, the cutting tool is engaged in the workpiece material; each cutting tooth composes an active part of the cutting tool, generating a local cutting force in the contact of the cutting region. This local cutting force varies depending on several parameters, such as chip thickness, region contact, specific cutting pressure, generated vibrations, etc. For this, to calculate the cutting forces applied on the complete cutting tool during the milling process, a mechanistic cutting force model of Altintas [18] is used. Moreover, the force is assumed to be proportional to the chip thickness (chip area) and axial depth of the cut (width of cut), respec–tively, corresponding to the cutting and edge forces. For a point on the (*jth*) cutting tooth, cutting force compo–nents respectively F_t, $F_r$and F_a is written as follows:

$$F_t = K_{tc}bh + K_{te}b \tag{1}$$

$$F_r = K_{rc}bh + K_{re}b \tag{2}$$

$$F_a = K_{ac}bh + K_{ae}b \tag{3}$$

where b is the width of the cut (axial depth), the length of an infinitesimal cutting tooth, h is the chip thickness, and K_{tc}, $K_{te}$and K_{rc}, K_{re} are the tangential and radial cutting force coefficients, depending on the workpiece material properties, tooth geometry, tool wear, and material temperature. Furthermore, the subscripts (k_c) and (k_e) represent cutting and edge force coefficients, respectively. Additionally, the third cutting force component $F_a$in axial direction (tool axis), is neglected due to its weak influence.

Further, the cutting force components can be rewritten for a point on the (*jth*) cutting tooth, where the differential milling forces corresponding to an infinitesimal axial depth of cut (dz) in the tangential F_t and radial $F_r$directions can be given as in the following:

$$F_{tj} = \left[K_{tc}h_j(\varnothing, z) + K_{te}\right]dz \tag{4}$$

$$F_{tj} = \left[K_{tc}h_j(\varnothing, z) + K_{te}\right]dz \tag{5}$$

after that, the differential cutting force components F_t and F_r are then transformed to Cartesian coordinate system x and y force components in the feed and normal direction respectively corresponding to F_x and F_y based on Figure 5 as shown in follows:

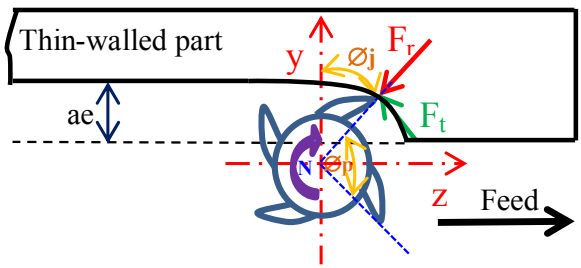

Figure 5. Differential cutting force components act on the cutting tool in the milling process.

$$F_y(\varnothing) = F_t\sin(\varnothing) - F_r\cos(\varnothing) \tag{6}$$

$$F_y(\varnothing) = F_t\sin(\varnothing) - F_r\cos(\varnothing) \tag{7}$$

where Ø: is the local tool immersion angle.

The cutting force components acting on the mill cut–ting tool in x and y directions for each tool immersion angle step are given as:

$$F_x = (\varnothing) = \sum_{i=1}^{K} \sum_{j=1}^{M} F_{x,j}(\varnothing) \quad (8)$$

$$F_y = (\varnothing) = \sum_{i=1}^{K} \sum_{j=1}^{M} F_{y_{i,j}}(\varnothing) \quad (9)$$

where K and M are the numbers of teeth and axial discs, respectively.

From the above formula, the two force components vary in magnitude and direction.

3.1 Chip thickness formulation

The chip thickness consists of a static part due to the rigid body motion of the cutting tool, while the workpiece is taken as a flexible body. The instantaneous chip thickness at a certain angular location angle on the cutting edge, which varies continuously during the milling, can be approximated as follows:

$$h_i(\varnothing, z) = f_z \sin \varnothing_i(z) \quad (10)$$

where f_z is the feed per tooth and $\varnothing_j(z)$ is the immersion angle for the tooth (j) at axial position z, taking the helical angle of tool tooth β into calculations.

3.2 Cutting tool engagement angles

The cutting tool engagement angles in the tool-part con–tact region depend on the type of milling operation and the tool and part geometry that can be calculated for up-milling operation by using the following expression (11).

$$\text{For Up milling} \quad \begin{cases} \varnothing_{st}(z) = 0 \\ \varnothing_{ex}(z) = \cos^{-1}\left(1 - \dfrac{ae}{R}\right) \end{cases} \quad (11)$$

where, the angles $\varnothing_{st}$ and $\varnothing_{ex}$ represent the beginning and the end of the cut, respectively, for each tooth engaged into the part material in each tool revolution.

3.3 Slicing the cutting tool

A numerical technique was used to obtain the cutting forces with accuracy, which slices the engaged part of the cutting tool into the material axially to a series of small discs with a uniform differential height dz depen–ding on tool engagement region limits [19]. Subse–quently, the cutting force contributions of each tooth of the cutting tool are calculated by additions for all segments of discs that are effectively in contact with the workpiece material at each cutting tool position of the scheduled tool path.

Next, the main step in the next subsection is to calculate $F^y(\varnothing)$ for each tooth along discretized axial cutting edges (sliced discs) at each tool path position.

3.4 Milling force calculation procedure

In this subsection, forces $F_y(\varnothing)$are determined against tool angles and per each axial elementary cutting edge, and therefore for full cutting contact region between the cutting tool and workpiece. Afterward, the calculated cutting forces should be transformed in order to be varied according to the machining time.

For this, a harmonic sinus force function is established, with a main amplitude F_{y0} presenting the average value of all calculated forces acting on elemen–tary cutting edges (discs) for each tooth passing the time. In addition to this, the time of passing of tooth τ in (12) is divided by the number of the created elementary edges (discs) to obtain small finite intervals of time for constant spindle speed N with a period $T=\tau$ for machining process stability.

$$\tau = \frac{60}{NZ} \quad (12)$$

with: t: Time of passing of toothbetween subsequent teeth of tool (s);

N: Spindle speed rotation (rpm);

Z: Number of teeth of the tool.

For more accurate calculations of the cutting force $F_y(\varnothing)$for each tool tooth, the following main steps of the below algorithm work as follows:

- For each tool position of a generated machining tool-path
- For each tooth of the tool
  - Determine the region engagement tool-workpiece [$\varnothing_{st}$, $\varnothing_{ex}$]with a fixed step tool angle.
  - Calculate the number of the elementary cutting edges (discs) according to the axial depth of the cut ap,
- For each disc from the bottom to the top of the cutting region of the tool through the created discs:
  - Calculate F_{y_disc}per each axial disc,
  - Calculate the total cutting force F_{y_total} by summations of all cutting force for all discs (F_{y_disc})
  - Calculate the average radial cutting force per disc ($F_{y0}=F_{y\_disc}$) by dividing the F_{y_total} by the number of the elementary cutting edges (discs),
  - Calculate the time of passing of tooth $\tau = \dfrac{60}{NZ}$
  - Dividing the τ by the number of the elementary cutting edges (discs) to obtain the incremental time Δt,
  - Creating the cutting force $F_{ytime}(t)$ depending on the machining time,
  - Creating a harmonic sinus force function in time as in the following expression:

    $F_y(t)=F_{y0}*sin(\omega_f*t)$ *for* $t \in [t_1:\Delta t:\ \tau]$

    With ω_f is the radial harmonic sinus force $F_y(t)$ *excitation frequency.*

Figure 6 summarizes the implemented algorithm of cutting force calculations against tool angles for each elementary axial cutting edge of a tool tooth.

Afterward, the next section will be dedicated to the prediction of thin-walled part displacement vibrations, which involves their modeling after calculating the generated cutting forces with accuracy for straight thin-walled geometry of workpieces and evaluating the surface roughness.

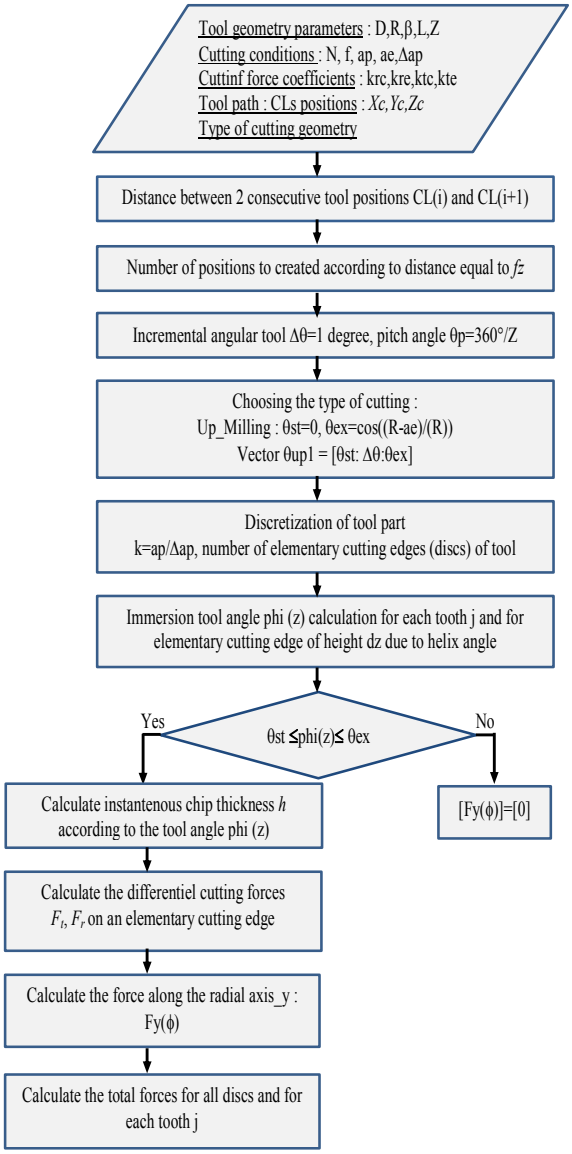

Figure 6. Algorithm of the cutting force per cutting tooth calculations.

4. MODELLING THIN-WALLED PARTS IN BENDING VIBRATIONS

4.1 Equation of motion of the thin-walled part

The thin-walled part is modeled as a cantilever beam, described by the differential equation of Euler-Bernoulli beam in forced bending vibrations subject to the exter–nal calculated cutting force F_y in the radial direction and acting at their free extremity which is given as in the following [20].

$$EI\frac{\partial^4 w(x,t)}{\partial x^4}+\rho S\frac{\partial^2 w(x,t)}{\partial x^2}=F_y(x,t),\forall x\in[0,L],t\geq 0 \quad (13)$$

Equation (13) is a partial differential equation expressed in space and time, corresponding to the fourth and second order, where *w(x, t)* is the bending displacement in the y-axis varied according to time *t* and located at a distance *x* along the beam's length *L*.

Afterward, $EI\frac{\partial^4 w(x,t)}{\partial x^4}$, and $F_y(x,y)$ are, respectively, the bending term [21] and the radial cutting force.

While *S*, *L*, ρ, and *I* are, respectively, the beam's cross-section, the beam, the length of the beam, the material mass density, and the moment of inertia for rectangular cross-sections. Furthermore, *EI* and ρS are, respectively, the flexural stiffness and the beam's mass divided by its length.

The main expression (13) can be written again as in the following form expression:

$$\Im\left(\frac{\partial^2 w}{\partial t^2}\right)+\mathcal{L}(w)=F_y(t)\delta(x-L) \quad (14)$$

Subsequently, the differential operators $\Im$ and $\mathcal{L}$ are, respectively, the mass operator with rearrangement and the stiffness operator, which are givenbelow [22].

$$J=\rho S \quad (15)$$

$$\mathcal{L}=EI\frac{d^4}{dx^4} \quad (16)$$

Using the Dirac operator δ, the term $F_y(t)\delta(x\text{-}L)$ is taken as an impulsive radial cutting force acting at $x=L$.

Next, the boundary conditions for the cantilevered beam are applied on the fixed and the free extremity, respectively, as in the following expressions [20]:

- Fixed-end beam:

$$x=0,\forall t: w(0,t)=0 \text{ and } \frac{\partial w(0,t)}{\partial x}=0 \quad (17)$$

- Free-end beam:

$$x=L,\forall t: EI\frac{\partial w^2(L,t)}{\partial x^2}=0 \text{ and } EI\frac{\partial^3 w(L,t)}{\partial x^3}=0 \quad (18)$$

4.2 Main steps of the solution method

Solving the equation of motion (13) in free bending vibrations involves $F_y(x,t) = 0$ to calculate the natural frequencies and their associated mode shapes in the radial direction of cut (y-axis) as follows:

$$EI\frac{\partial^4 w(x,t)}{\partial x^4}+\rho S\frac{\partial^2 w(x,t)}{\partial t^2}=0 \quad (19)$$

The separation method of variables is employed to calculate the general solution, which gives the displa–cement of the thin-walled part taken as a summation of modal responses as follows:

$$w(x,t)=q_n(t),\varnothing_n(x) \quad (20)$$

With the generalized coordinates and the mode shape expression of *n* mode, the order corresponds to $q_n(t)$ and $\phi_n(x)$, respectively.

Resolving (19) consists of replacing the general solution (20) within (19) by obtaining two different ordinary differential equations (21) and (22) in time and spatial given, respectively [20].

$$\frac{\partial^2 q(t)}{\partial t^2}+\omega^2 q(t)=0 \quad (21)$$

$$EI\frac{\partial^4\phi(x)}{\partial x^4}-\omega^2\left(\rho S\phi(x)\right)=0 \tag{22}$$

Assuming that the temporal solution $q(t)$ is given by a sinusoidal form while the spatial solution $\varnothing(x)$ is expressed by both sinusoidal and hyperbolic functions as in the following [23]:

$$q(t)=d_1\sin\omega t+d_2\cos\omega t \tag{23}$$

$$\varnothing(x)=C_1\sin ax+C_2\cos ax+C_3\sinh ax+C_4\cosh ax \tag{24}$$

The constants of integration(d_1, d_2) and (C_1, C_2, C_3, C_4) are calculated respectively according to the fixed initial conditions and the applied boundary conditions.

To obtain the spatial solution of the ordinary diffe–rential equation (22), the mode shape (24) should be substituted into (22) that meets the boundary conditions (17) and (18), allowing the calculation of the mode shapes as in (25) and the natural frequency in (28) by the below expressions [20]:

$$\varnothing_n(x)=\cosh a_n x-\cos a_n x-\gamma_n\left(\sinh a_n x-\sin a_n x\right) \tag{25}$$

with:

$$\gamma_n=\frac{\cos(a_n l)+\cosh(a_n l)}{\sin(a_n l)+\sinh(a_n l)} \tag{26}$$

$$a_n l=\frac{(2n-1)\pi}{2} \tag{27}$$

$$\omega_n=\left[k_{nl}\right]^2\sqrt{\frac{EI}{mL^4}} \tag{28}$$

Afterward, ω_n are the undamped natural frequencies of n mode order, L is the beam's length, $E$is Young's modulus, I is the moment inertia of cross-section, m is the mass per unit length, and then the initial values of $[k_{nl}]$ are provided by [20].

To solve the forced bending motion in (29), cutting force $F_y(t)$ is integrated, which is taken into calculations as a random force, utilizing the modal superposition method and the convolution theorem for the resolution. Hence, the radial displacement $w(x,t)$, which named the general solution as in (30), is indicated as a summation of modal responses as below:

$$EI\frac{\partial^4 w(x,t)}{\partial x^4}+\rho S\frac{\partial^2 w(x,t)}{\partial t^2}+F_y(x,t) \tag{29}$$

$$w(x,t)=\sum_{n=1}^{\infty}q_n(t),\varnothing_n(x) \tag{30}$$

By applying the orthogonality conditions to the mode shape expressions $\phi_n(x)$ in (25), the generalized mass M_n and the generalized stiffness K_n both associated with each mode n are given by the following expres–sions (31) and (32), respectively:

$$M_n=\int_0^1\rho S\varnothing_n^2(x)dx \tag{31}$$

$$K_n=\int_0^1\varnothing_n(x)EI\frac{d^4\varnothing(x)}{dx^4}dx \tag{32}$$

Replacing the general solution in (30) into (29) with including the orthogonality conditions, the undamped modal equation of motion is given as in following:

$$M_n\ddot{q}_n(t)+K_n q_n(t)=F_{yn}(t),\quad n=1,2,... \tag{33}$$

with $F_{yn}(t)$ represents the modal cutting force in a radial direction related to the mode shape of order n exerted at $x=L$ which is given as follows:

$$F_{yn}(t)=F_y(t)\int_0^l\varnothing_n(x)\delta(x-L)dx=F_y(t)\varnothing_n(L) \tag{34}$$

Therefore, the general solution which matches Du–hamel's integral formulation for the damped equation of motion under the action of the cutting force $F_{yn}(t)$ is given in the following expression [22]:

$$q_n(t)=\frac{1}{M_n\omega_d}\int_0^t F_{yn}(\tau)e^{-\xi\omega_n(t-\tau)}\sin\omega_d(t-\tau)d\tau \tag{35}$$

with $F_{yn}(\tau)$ is taken as an impulsive cutting force acting at a very short time which is the unknown variable provided by the results of the cutting force modeling method. Afterward, the damped natural frequency expression ω_d is given by including the structural damping ratio of part x, as in below:

$$\omega_d=\omega_n\sqrt{1-\xi^2} \tag{36}$$

4.3 Numerical estimation of the integral of Duhamel

The integral of Duhamel (37) should be evaluated nu–merically to calculate the general response utilizing multiple integrations by parts, as in the following form:

$$R_{ZMax}=Max\left(R_z(i)\right),i=1:5 \tag{37}$$

Estimating the integrals $A_n(t)$ and $B_n(t)$ numerically implies that the integral of Duhamel is calculated [22].

Then, the cutting force $F_{yn}(\tau)$ is taken as successions of sets of impulsive forces performed on short time intervals dτ as in below [23]:

$$F_{yn}(\tau)=F_{yn}(t_{i-1})+\frac{\Delta F_{yn}}{\Delta t_i}(\tau-t_{i-1}),\ t_{i-1}\le\tau\le t_i \tag{38}$$

Including (38) into other integrals calculations, where the integral formulation of the beam is written regarding the time $t_i$as in below [23]:

$$q_n(t_i)=\frac{1}{M_n\omega_n}\left\{A_n(t_i)\sin\omega_n t_i-B_n(t_i)\cos\omega_n t_i\right\} \tag{39}$$

Substituting the formulation in (39) into the radial displacement expression (30) located at$x=L$ (free-end extremity) and for each incremented time t_i the follo–wing expression is obtained:

$$w(L,t_i)=\sum_{n=1}^{\infty}q_n(t_i)\varnothing_n(L) \tag{40}$$

Figure 7 shows the flowchart that summarizes the analytic method for displacement vibration calculations.

The next section will be dedicated to finite element simulations in bending vibrations.

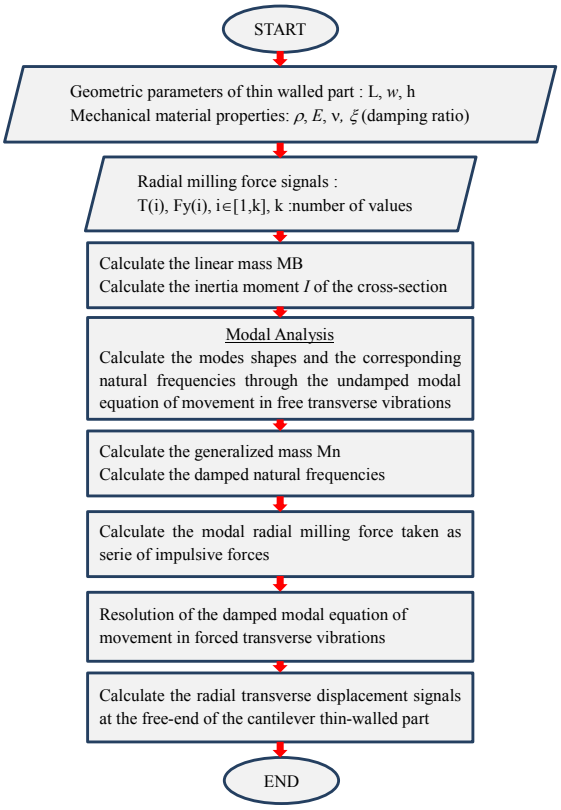

Figure 7. Flowchart of the analytic displacement modeling.

5. NUMERICAL SIMULATIONS VIBRATIONS USING FE METHOD

5.1 Finite element method simulation in bending vibrations

The CAD model of the thin-walled part is sketched into the Comsol Multiphysics environment with their dimensions. Afterward, the calculated forces $F_y(t)$ obtained from the milling force modeling under some cutting conditions are introduced as cutting force excitations. Then, for a sketched cantilever thin-walled part introducing their appropriate mechanical materials properties, the CAD model is approached by their discretization to the finite number of volumetric elements. Afterward, one extremity of the thin-walled part has been constrained in displacements and rotations through all areas of their cross-section. Then, modal analysis is applied to the geometric model to compute the mode shapes with their corresponding Eigenfrequencies. Finally, the forced displacement vibrations are determined by exciting its free extremity by the different cutting forces obtained under certain milling conditions.

6. SIMULATION RESULTS

6.1 Simulation conditions for cutting force calculations

This subsection gives the following conditions for running the analytical simulations of cutting forces. The flat milling tool comprises four cutting edges applied in the up-milling process. Afterward, the necessary mechanical properties of the cantilever thin-walled part are listed in Table 1. Then, the geometrical solid cutting tool values are: L_t=120 mm, D=12 mm, Z=4 teeth, β=35°, and its material is the carbide. The part's dimensions are: length of part L=130 mm, width w=50 mm, thickness h=5 mm, and its material is aluminum alloy 7050. Then, the used machining conditions are fixed at the beginning as in the following: ap=2 mm,ae=0.5 mm,fz=0.08 mm/tooth, f=480 mm/min, and with an incremental elementary axial depth of cut Δap=0.2 mm. At the same time, the rotational spindle speed is taken equal to N=1500 rpm with the determined tool revolution period equal to τ=0.01 s. In addition, the tangential and radial cutting and edge force coefficients are also given respectively [24]: K_{tc}=1282.31N/mm^2, K_{te}=4.34 N/mm, K_{rc} = 579.16 N/mm^2, K_{re}=5.38 N/mm for a given combination couple of cutting tool and workpiece material, tool geometry and so on. Moreover, the aluminum alloy's structural damping ratio is equal to ξ=1.5% [25].

Table 1 Mechanical material property values of part [25].

Mechanical Property	Variable	Value
Young's Modulus (N/mm^2)	E	7.03E+10
Density (Kg/m^3)	ρ	2830
Poisson's ratio	ν	0.33

Afterward, the tool path positions are generated by fixing the distance between two consecutive tool positions equal to fz. Then,forces $F_y(\varnothing)$are calculated at each elementary axial cutting edge and, afterward, for each tool tooth according to each tool position.

6.2 Results Verification and Discussions

In this subsection, the cutting forces per tooth are calculated by summating the forces exerted at each elementary axial cutting edge, which are presented and analyzed in the following. In addition, the calculated displacement vibrations and, consequently, the corresponding calculated machined surface roughness parameters are presented and analyzed next. For this, some case studies according to variations of the ae parameter are presented below through the proposed analytical method and the numerical simulations.

Case study 1: ae=0.5 mm

7.2.1 Cutting force determination

The first results are focused on the cutting forces calculated analytically according to the tool angle variations and then according to engagement times of each cutting edge tooth along the scheduled tool path (some tool positions are taken for more clarity and details). Secondly andfor more details, calculated cutting forces depending on the tool angle are transformed into temporal forces. Once forces $F_y(\varnothing)$are calculated, then their average F_{y0} is determined, and it is equal to F_{y0}=37.09 N per each axial cutting edge. In the next, the value of F_{y0} is integrated into transformation to obtain a harmonic temporal sinusoidal force $F_y(t)$ defined by a trigonometric function according to the machining time, which is used as an excitation cutting force. Subsequently, the radial displacement at the free end of the cantilever thin-walled part is calculated along three tool revolutions. After that, Figure 8 (a-b) shows,

respectively $F_y(\varnothing)$ and $F_{ytime}(t)$ taken with a period of time equal to τ=0.01 s. While Figure 9 shows the cor–responding harmonic sinusoidal radial force signal $F_y(t)$ generated with an excitation frequency ω_f=1000 Hz.

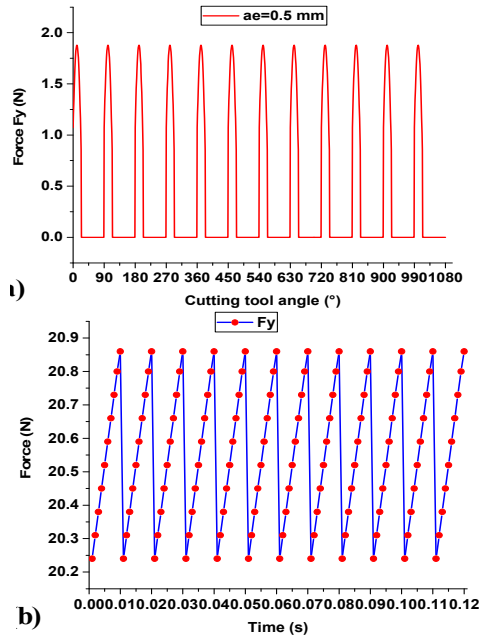

Figure 8. Fymagnitude against (a) Tool angles (degree) (b) Time of machining (s), for ae=0.5 mm, ap=2 mm, fz=0.08 mm/tooth, f=480 mm/min and N=1500 rpm.

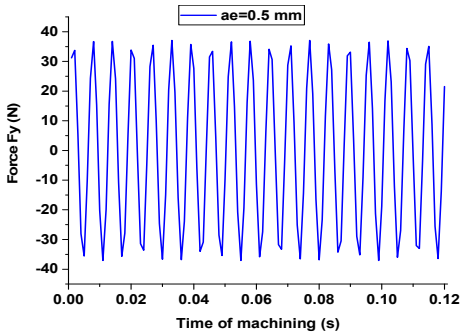

Figure 9. Radial harmonic sinus force $F_y(t)$generated with an excitation frequency ω_f=1000 Hz, for ae=0.5 mm, ap=2 mm, fz=0.08 mm/tooth, f=480 mm/min and N=1500 rpm.

7.2.2 Displacement calculations from analytical cutting force modeling

Next, once $F_y(\varnothing)$ signal is calculated, it is inputted into another program to calculate the corresponding displa–cement vibration, as shown in Figure 10.

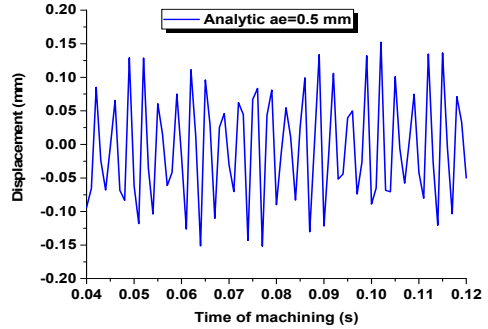

Figure 10. Analytic displacement versus machining time for ae=0.5 mm, ap=2 mm, fz=0.08 mm/tooth, f=480 mm/min, and N=1500 rpm.

7.2.3 Displacement computation from finite element (FE) simulations

They use the finite element method (FE) in dynamic simulations with the Comsol Multiphysics software, where the thin-walled part is sketched using the same mechanical properties of the workpiece material men–tioned above. Subsequently, the force signal $F_y(t)$is in–corporated into the software environment and is applied to excite the free end of the cantilever thin-walled part to compute the corresponding radial displacement signal. Then, the different steps to compute the transverse radial displacement vibrations are illustrated in the following order, as shown in Figure 11.

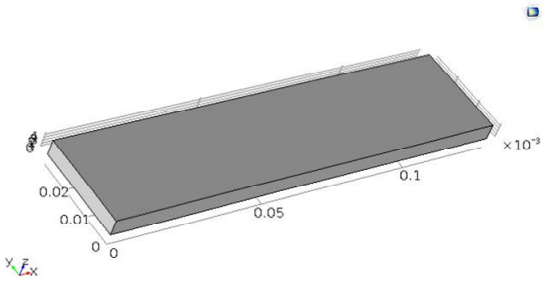

(a) CAD model of thin-walled part with all dimensions.

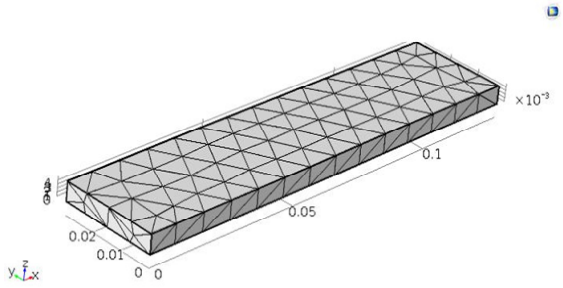

(b) Meshing the CAD model.

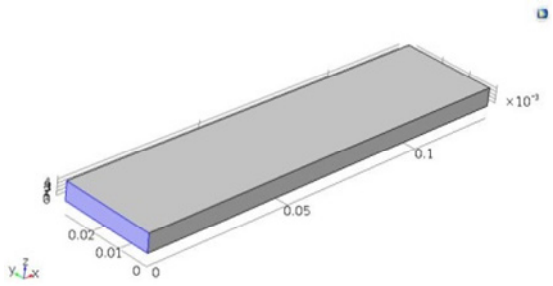

(c) Fixed constraint at the left side end.

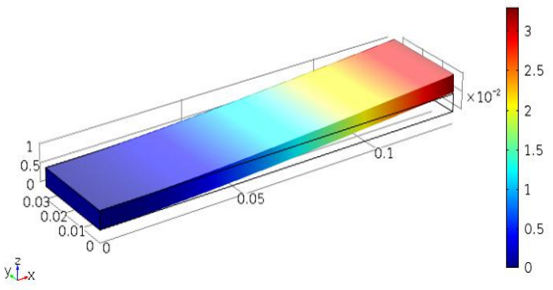

(d) First bending mode shape of the cantilever thin-walled part.

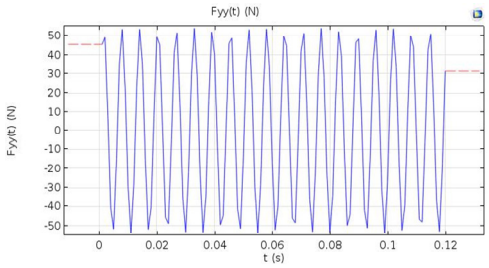

(e) Harmonic sinus cutting force excitation in time.

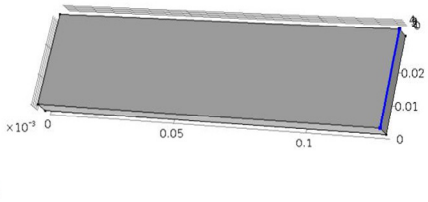

(f) Applying the excitation force signal at the free end.

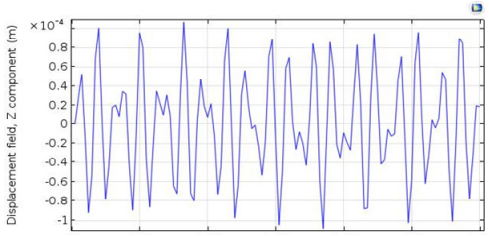

(g) Computed radial displacement vibration.

Figure 11. Steps of the computations using finite element (FE) simulations, for ae=0.5 mm, ap=2 mm, fz=0.08 mm/tooth, f=480 mm/min, and N=1500 rpm.

7.2.4 Analytical and numerical radial displacements comparison

To verify the displacement results from issues from the analytical approach, a comparison is performed between the analytical and computed displacement, as depicted in Figure 12, taken as an example. The analysis shows that the two types of displacement are close in magnitude and profile trend.

To evaluate the machined surface quality when milling the thin-walled part from displacements, some main surface amplitude parameters are presented by defining them as in the following such as roughness average (R_a), root-mean-square roughness (R_q), the ma–ximum height of peak-to-valley roughness (R_z or R_{ZMax}) andR_v.

- R_a (average roughness)

$$R_a = \frac{|Z_1(x)| + |Z_2(x)| + \ldots + |Z_n(x)|}{n} \tag{41}$$

- *Rzaver* (peaks and valleys) and R_{ZMax}

R_{zaver} and $R_{ZMax}$are calculated after relevant points of peak-deepest valley graph from displacement against time per a sampling length l_r.

$$R_z(1) = |g(1)| + |g(2)| \text{ per asampling length } l_r \tag{42}$$

$$R_{zaver} = \frac{R_z(1) + R_z(2) + R_z(3) + R_z(4) + R_z(5)}{5} \tag{43}$$

$$R_{ZMax} = Max\left(R_z(i)\right), i = 1:5 \tag{44}$$

- R_{qaver}: for total evaluation length

$$R_{qaver} = \frac{Z_1^2(x) + Z_2^2(x) + \ldots + Z_n^2(x)}{n} \tag{45}$$

- $Rv=|Min\ (Z(x))|$Maximum profile valley depth indicates the point along the sampling length at which the profile curve of displacement is lowest.

R_v: is calculated for five values of the valley deepest per same sampling length.

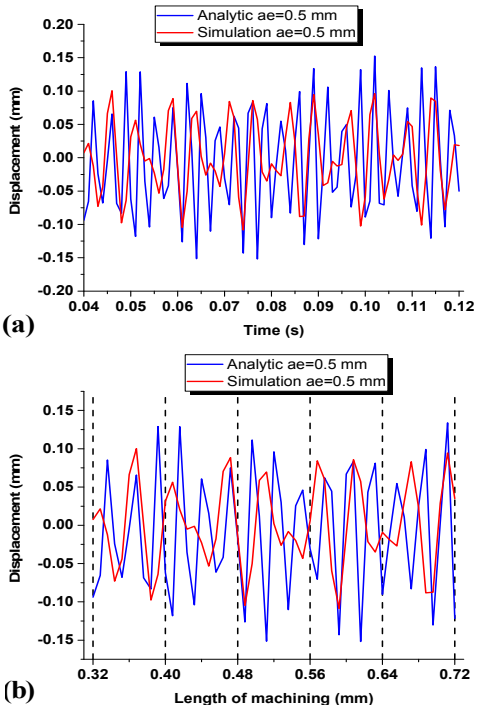

Figure 12. Comparisons between radial displacement obtained by analytical and numerical simulation against (a) Time of machining (b) Length of machining both, with ae=0.5 mm, ap=2 mm, fz=0.08 mm/tooth, f=480 mm/min, N=1500 rpm.

$$R_v = \left|Min\left(Z(x)\right)\right| \text{ per asampling length } l_r \tag{46}$$

7.2.5 Roughness topography evaluation from two types of displacements

Afterward, once the two types of radial displacement vibrations are determined, the roughness parameters of the machined surface finish are calculated based on the analytical and computed displacements. Hence, Figures 13(a) and 13(b) show 3D roughness R_a values plotted against the fixed length of machining (z-axis) and along the discretized axial depth of cut(Δap) (x-axis).

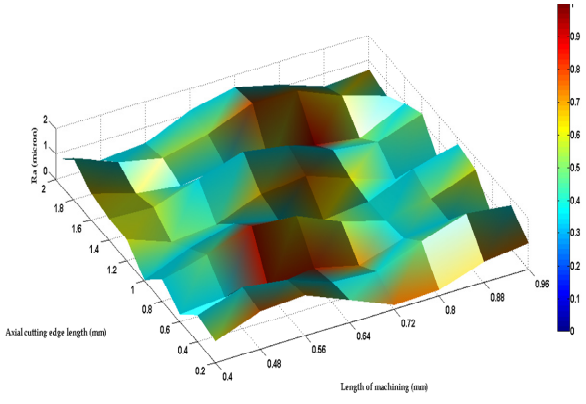

a)

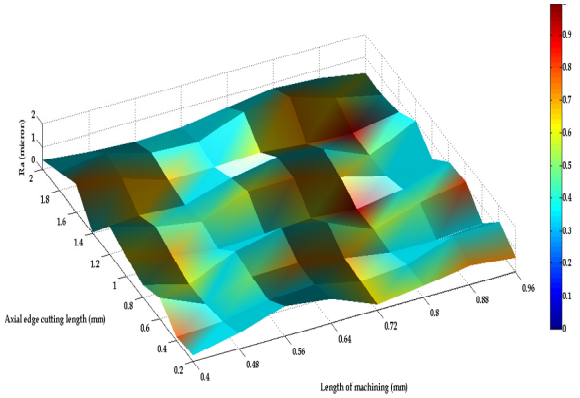

b)

Figure 13. 3D Roughness topography Ra based on radial displacement for (a) Analytical modeling (b) Simulation with Comsol Multiphysics.

Subsequently, Figure 14 (a-b) shows the truncated radial displacement versus the length of machining for two consecutive cutting tool revolutions that correspond to the interval [0.32mm-0.72mm] for the analytical method and the numerical simulation. Then, the surface roughness parameters are calculated.

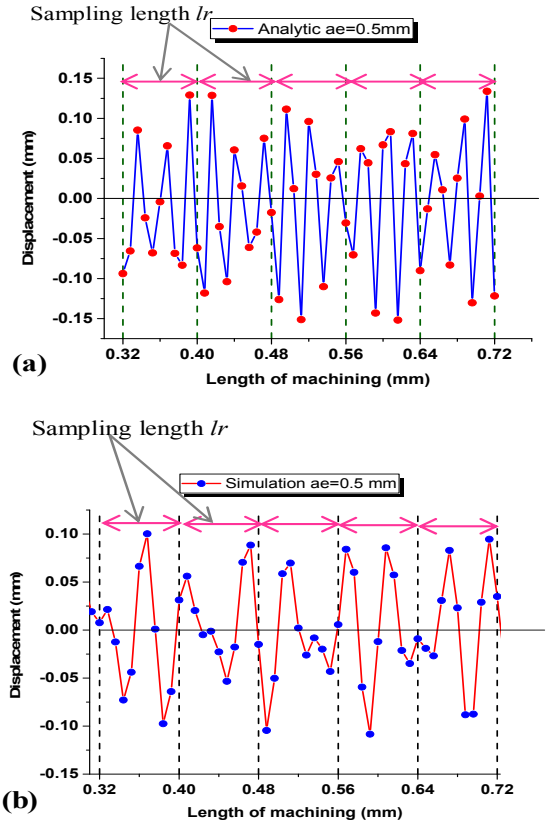

Figure 14. Transverse displacement against the machining length obtained from (a) Analytic modeling and (b) Comsol Multiphysics software computation.

Next, Table 2 recapitulated the calculated values of the surface roughness parameters R_a, R_{zaver}, R_{ZMax}, R_q, and $R_v$obtained from the proposed two methods and is not from the comparative point of view.

In that case, the parameter *ae* involves new changes in their values, which are used for another new successive peripheral milling passes to recalculate and to compare the new averaged F_{y0} for the two methods.

$$ae = ae\_nominal \pm \frac{R_a}{2}$$
$$ae = ae\_nominal \pm \frac{R_q}{2} \quad (47)$$
$$ae = ae\_nominal \pm \frac{R_v}{2}$$

Table 2 Surface roughness parameters obtained by analytical and FEM simulations for ae=0.5 mm.

ae=0.5 (mm)	***Ra*** (μm)	***Rzaver*** (mm)	R_{ZMAX} (mm)	***Rq*** (RMS) (mm)	***Rv*** (mean 5 values) (mm)
Analytic	70.01	0.2442	0.2641	0.0672	0.1270
FEM Simulations	44.97	0.1782	0.1977	0.0450	0.1084

Subsequently, Table 3 summarizes the calculated average cutting forceF_{y0}per each axial cutting edge of the tool with their corresponding variations of the parameter *ae*=0.5 mm for the analytical modeling and the numerical simulations using the FE method.

Table 3 Effect of ae parameter variations on the average force per tooth calculations for ae=0.5 mm, ap=2 mm, fz=0.08 mm/tooth, f=480 mm/min, N=1500 rpm.

	From Analytical Modelling		From Numerical Simulation using (FE)	
ae Variations (mm)	ae_new (mm)	F_{y0Anal} (N)	ae_new (mm)	F_{y0FEM} (N)
ae=0.5	0.5	37.09	0.5	37.09
ae=0.5+R_a/2	0.535	37.79	0.523	37.79
ae=0.5-R_a/2	0.465	36.21	0.478	37.09
ae=0.5+R_q/2	0.534	37.79	0.523	37.79
ae=0.5-R_q/2	0.466	36.21	0.478	37.09
ae=0.5+R_v/2	0.564	38.31	0.446	36.21

	Evaluation
ae Variations (mm)	Err=|[(F_{y0FEM}-F_{y0Anal})/ F_{y0FEM}]|*[100] (%)
ae=0.5	0
ae=0.5+R_a/2	0
ae=0.5-R_a/2	2.43
ae=0.5+R_q/2	0
ae=0.5-R_q/2	2.43
ae=0.5+R_v/2	5.48

The main analysis of Table 3 shows that the error of the force difference is high at 5.48 % when incor–porating +R_v/2 into calculations. In contrast, no difference (zero error) is noticed for the value of *ae* parameter when +R_a/2 and +R_q/2 are added.

7.2.6 Roughness parameters prediction from two types of displacements under the influence of ae variations

Case study 2: ae=2.5 mm

In the second part of the study, the nominal value of *ae* is taken high(*ae*=2.5 mm) to show their effect on the roughness parameters of the machined surface-precisely the surface marks left by the last teeth of the cutting tool. For this, the machining conditions for running

cutting force calculations are the following: *ae*=2.5 mm, *ap*=2 mm, *N*=1500 rpm, *fz*=0.1 mm/tooth, and *f*=600 mm/min. For the evaluation, a comparison is performed between displacements obtained from the two different methods, as depicted in Figure 15, which are close.

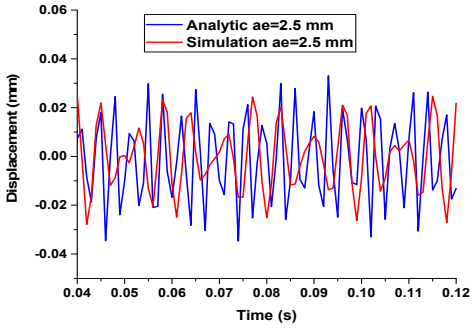

Figure 15. Radial displacements comparison between the two methods, with ae=2.5 mm, ap=2 mm, fz=0.10 mm/tooth,f=600 mm/min, N=1500 rpm.

Next, the calculated corresponding main surface roughness parameters are shown in Table 4.

Table 4. Roughness parameters obtained by analytical and FEM simulations ae=2.5 mm.

ae=2.5 mm	*Ra* (μm)	*Rzaver* (mm)	R_{ZMAX} (mm)	*Rq* (RMS) (mm)	*Rv* (mean 5 values) (mm)
Analytic	215.6	0.6706	0.7354	0.2536	0.3490
FEM Simulations	119.63	0.3918	0.4886	0.1456	0.2057

Case study 3: ae=0.5 mm

For the same machining conditions, a new second peripheral milling pass is performed with *ae*=0.5 mm successive to the first machining pass (*ae*=2.5 mm). Then, by taking into account the last calculated roughness parameter values as in Table 4, the new *ae*_new is recalculated, and therefore their effect on the average cutting force F_{y0} is evaluated.

Table 5. Surface roughness parameters values obtained from displacements by analytical and FEM simulations for ae=0.5 mm.

ae=0.5 mm	*Ra* (μm)	*Rzaver* (mm)	R_{ZMAX} (mm)	*Rq* (RMS) (mm)	*Rv* (mean 5 values) (mm)
Analytic	14.4	0.0797	0.0891	0.0215	0.03915
FEM Simulations	9.5	0.0665	0.0736	0.0153	0.03113

Table 6. Effect of ae variations on the average force F_{y0}calculations for ae=0.5 mm.

	From Analytical Modelling		From Numerical Simulation using (FE)	
ae Variations (mm)	ae_new (mm)	F_{y0Anal} (N)	ae_new (mm)	F_{y0FEM} (N)
ae=0.5	0.5	37.09	0.5	37.09
ae=0.5+R_a/2	0.6078	38.63	0.5598	37.79
ae=0.5-R_a/2	0.3922	34.03	0.4402	36.21
ae=0.5+R_q/2	0.6268	38.63	0.5728	38.31
ae=0.5-R_q/2	0.3732	34.00	0.4272	35.18
ae=0.5+R_v/2	0.6745	38.74	0.6029	38.31

	Evaluation
ae Variations (mm)	Err=|[(F_{y0FEM}-F_{y0Anal})/ F_{y0FEM}]|*[100] (%)
ae=0.5	0.00
ae=0.5+R_a/2	2.22
ae=0.5-R_a/2	6.02
ae=0.5+R_q/2	0.84
ae=0.5-R_q/2	3.35
ae=0.5+R_v/2	1.12

Therefore, Table 5 summarizes the calculated surface roughness parameters, while Table 6 summarizes and compares the calculated cutting force F_{y0} according to *ae* variations based on the two presented methods.

The main remark that can be drawn from this evaluation is that the lowest error is found, about 0.84% for $+R_q/2$, while the error is high, about 6.02% for $-R_a/2$.

Case study 4: ae=0.75 mm

In this case, the value of *ae* is taken equal to 0.75 mm for a second new peripheral milling pass, performed after the first peripheral milling pass with *ae*=2.5 mm keeping fixed the same machining conditions. As a result, Tables 7 and 8 recapitulate both the surface roughness parameters and averaged cutting force F_{y0} values.

The principal remark that can be drawn while increasing the variations of the parameter *ae* from 0.5 mm to 0.75 mm on F_{y0} is that a notified difference equal to 2.23 % when adding $R_a/2$ and $R_q/2$. In contrast, a difference is almost close to zero when -R_a/2 and R_q/2 are added. In conclusion, R_a and R_q have the same influence; while adding $+R_v/2$, the error is about 5.17%according the changes for F_{y0}.

Table 7. Surface roughness parameters values obtained from displacements by analytical and FEM simulations for ae=0.75 mm.

ae=0.75mm	*Ra* (μm)	*Rzaver* (mm)	R_{ZMAX} (mm)	*Rq* (RMS) (mm)	*Rv* (mean 5 values) (mm)
Analytic	74.14	0.2452	0.2737	0.07	0.123
FEM Comsol	43.68	0.1582	0.1922	0.0422	0.0721

Table 8. Effect of ae variations on the average force F_{y0}calculations for ae=0.75 mm.

	From Analytical Modelling		From Numerical Simulation using (FE)	
ae Variations (mm)	ae_new (mm)	F_{y0Anal} (N)	ae_new (mm)	F_{y0FEM} (N)
ae=0.75	0.75	38.63	0.75	38.63
ae=0.75+R_a/2	0.8578	36.86	0.8098	37.70
ae=0.75-R_a/2	0.6422	38.63	0.6902	38.74
ae=0.75+R_q/2	0.8768	36.86	0.8228	37.70
ae=0.75-R_q/2	0.6232	38.63	0.6772	38.74
ae=0.75+R_v/2	0.9245	35.75	0.8529	37.70

	Evaluation
ae Variations (mm)	$Err=\|[(F_{y0FEM}-F_{y0Anal})/ F_{y0FEM}]\|*[100]$ (%)
ae=0.5	0.00
ae=0.5+R_a/2	2.23
ae=0.5-R_a/2	0.28
ae=0.5+R_q/2	2.23
ae=0.5-R_q/2	0.28
ae=0.5+R_v/2	5.17

7. CONCLUSIONS

The paper presents the surface roughness parameters of thin-walled parts calculated based on the maximum displacement vibrations at their top free-end excited by the cutting tooth edge force along generated straight tool paths during peripheral milling. Based on the utilized mechanistic cutting force, machining conditions, tool geometry, type of material, and tool path are integrated into the calculations. Then, analytical modeling using Euler-Bernoulli beam theory and finite element (FE) simulation using the Comsol multiphysics software are performed for the bending vibrations of thin-walled parts. The influence of the parameter *ae* on the flexible cantilevered part is searched to adjust the values of *ae* under fluctuations of the surface roughness caused by the cutting edge of teeth of the flat-end milling tool. Surface roughness parameters (R_a, $R_q$and R_v) are calculated for successive machining passes, which can contribute to keeping cutting forces fixed during machining and consequently maintaining the machined surface quality stable as possible.

It is concluded that the surface roughness parameters $\pm R_a$ and $\pm R_q$ lead almost to the same tendency according to the generation of cutting forces with minimum errors against+$R_v$which its errors are high and relevant. In addition, it can be concluded in this paper that a part of the chatter that occurred during machining is indirectly included through *ae* changing. Finally, the developed approaches for bending vibrations and cutting force prediction help to predict and correct chatter marks left on the part surfaces from the teeth of the cutting tool, thus leading to the production of surface parts with uniform waviness regularities.

Further research can be extended for other part geometries with different materials and for several engagement times of passing of tooth, and then including experimental measurements.

The obtained results from this research method can be applied and extended for other main practical applications, such as online monitoring of surface roughness quality of components based on cutting force and displacement signals measurements for the cutting tool and the part to be machined. Furthermore, it can be applied to micro-milling parts with tight tolerances. Further detailing, the part's surface roughness is predicted indirectly based on displacement calculations caused by the acquired cutting force signal. In contrast, the surface roughness of the machined part can be calculated directly from the measured displacement vibration signal. Finally, this approach can be limited to only one sensor for real-time monitoring of CNC machiningand can help avoid using multiple sensors that should be installed on the machine tool.

REFERENCES

[1] Ma, J. Zhang, D. Wu, B et al.: Stability improvement and vibration suppression of the thin-walled workpiece in milling process via magnetorheological fluid flexible fixture. Int J Adv Manuf Technol, 88: pp.1231-1242, 2017.

[2] Yan, B., Zhu, L., and Liu, C.: Prediction model of peripheral milling surface geometry considering cutting force and vibration.Int J Adv Manuf Technol, Vol. 110, pp.1429-1443, 2020.

[3] Yao, Q., Luo, M., Zhang, D., Wu, B.: Identification of cutting force coefficients in machining process considering cutter vibration. Mech Syst Signal Process, Vol. 103:pp.39-59, 2018.

[4] Sun, W., Luo, M., and Zhang, D.: Machining vibration monitoring based on dynamic clamping force measuring in thin-walled components milling.Int J Adv Manuf Technol, Vol. 107. No 5, pp. 2211-2226, 2020.

[5] Wang, J., Ibaraki, S., Matsubara, A., Shida, K., Yamada, T.: FEMbased simulation for workpiece deformation in thin-wall milling.Int J Autom Technol, Vol. 9, pp. 122–128, 2015.

[6] Yue, C., Chen, Z., Liang, SY., et al. : Modeling machining errors for thin-walled parts according to chip thickness. Int J Adv Manuf Technol, Vol. 103, pp. 91-100, 2019.

[7] Fei, J., Lin, B., Yan, S., et al. : Modeling of surface roughness for manufactured thin-walled structure. Proc IMechE Part B: J Engineering Manufacture, Vol. 233, pp. 1216-1223, 2019.

[8] Shi, J., Gao, J., Song, Q., et al.: Dynamic deformation of thin-walled plate with variable thickness under moving milling force. Procedia Cirp, Vol. 58, pp. 311-316, 2017.

[9] Fei, J., et al.: Theoretical prediction and experimental validation of dynamic deformation during machining of thin-walled structure. In: ASME International Mechanical Engineering Congress and Exposition. American Society of Mechanical Engineers, V002T02A004, 2017.

[10] Zhang, L., et al.: Prediction of dynamic milling stability considering time variation of deflection and dynamic characteristics in thin-walled component milling process. Shock Vib, pp. 1-14, 2016.

[11] Bolar, G., and Joshi, SN.: Three dimensional numerical modeling, simulation and experimental validation of milling of a thin-wall component. Proc IMechE Part B: J Engineering Manufacture,Vol. 23, pp. 792-804, 2017.

[12] Khandagale, P., et al.: Modelling time-domain vibratory deflection response of thin-walled cantilever workpieces during flank milling. Journal of Manufacturing Processes, Vol. 33, pp. 278-290,2018.

[13] Masmali, M., Mathew, P.: An analytical approach for machining thin-walled workpieces. 16th CIRP Conference on Modelling of Machining Operations, Procedia CIRP, Vol. 58, pp. 187-192, 2017.

[14] Chen, W., Xue, J., Tang, D., et al.: Deformation prediction and error compensation in multilayer milling processes for thin-walled parts. Int J Mach Tools Manuf, Vol. 49, pp. 859-864, 2009.

[15] Globocki-lakić, Gordana, Sredanović, B., Jotić, G., et al. A comparative analysis of milling strategies of complex geometry surfaces.FME Transactions, 2022, vol. 50, no 4, p. 623-634.

[16] Zeng, S., Wan, X., Li, W., et al.: A novel approach to fixture design on suppressing machining vibra–tion of flexible workpiece. Int J Mach Tools Manuf, Vol. 58, pp. 29-43, 2012.

[17] Dun, Y., Zhu, L., and Wang, S.: Investigation on milling force of thin-walled workpiece considering dynamic characteristics of workpiece. J Mech Sci Technol, Vol. 33, pp. 4061-4079, 2019.

[18] Altintas, Y.: Manufacturing automation metal cut–ting mechanics machine tool vibrations and CNC design. 1st ed. Cambridge University Press, 2000.

[19] Abainia, S., Bey, M. : Integrated Dexels Geometric Model and Predictive Force Model for Feedrate Opti-mization in 03 Axis Milling Machine. Applied Mec–hanics and Materials, Vol. 372, pp. 377-380, 2013.

[20] Rao, SS.: Vibrations of continous systems. Wiley, New York, 2007.

[21] Han, S.M., Benaroya, H. and Wei, T.: Dynamics of transversely vibrating beams using four engineering theories. Journal of Sound and vibration, Vol. 225, pp. 935-988, 1999.

[22] Abainia, S., Ouelaa, N.: Predicting the dynamic be-haviour of the turning tool vibrations using an experimental measurement, numerical simulation and analytical modelling for comparative study. Int J Adv Manuf Technol, Vol. 115, pp. 2533-2552, 2021.

[23] Abainia, S., Ouelaa, N., and Djamaa, MC.: Modeling and experimental validation of dynamic response of the cutting tool in turning operations. FME Transactions, Vol 48, pp. 454-459, 2020.

[24] Shi, K., Liu, N., Wang, S., and al.: Effect of tool path on cutting force in end milling. Int J Adv Manuf Technol, Vol. 104, pp. 4289-4300, 2019.

[25] Yang, Y. et al. : Residual stress relaxation of thin-walled long stringer made of aluminum alloy 7050-T7451 under transportation vibration. Chin J Mech Eng, Vol. 33, pp.1-10, 2020.

NOMENCLATURE

ae	radial depth of cut
ae_new	updated radial depth of cut added with roughness parameter value
dz	infinitesimal axial depth of cut
F_t	differential tangential cutting force per infinitesimal axial depth of cut
F_r	differential radial force per infinitesimal axial depth of cut
F_a	differential axial force per infinitesimal axial depth of cut
$F_x(\varnothing)$	cutting force in the feed direction at each tool immersion angle ∅
$F_y(\varnothing)$	cutting force in the normal direction at each tool immersion angle ∅
F_{y_disc}	average radial cutting force per an axial disc (elementary cutting edge)
F_{y0}	average radial cutting force per an axial disc (elementary cutting edge)
$F_{v\ total}$	the total radial cutting force of all axial discs
$F_{ytime}(t)$	radial cutting force according to the machining time t
$F_y(t)$	radial harmonic sinus force function in time
$F_{yn}(t)$	radial harmonic sinus force function in time of order n
$F_{yn}(\tau)$	impulsive radial harmonic sinus force function of order n
$F_y(t)\delta(x\text{-}L)$	impulsive harmonic sinus force function in time acted at $x=L$
F_{y0Anal}	average radial cutting force per each axial disc obtained by analytical method
F_{y0FEM}	average radial cutting force per each axial disc obtained by finite element
$F_y(x,t)$	spatiotemporal radial cutting force
j^{th}	cutting tooth number
K	number of teeth of the mill-cutting tool
k	number of axial discs of the tool
K_n	generalized stiffness associated with each mode n
M	number of axial discs of the mill cutting tool
M_n	the generalized mass associated with each mode n
N	spindle speed
T	period of the spindle
$w(x, t)$	bending radial displacement (y-axis)
Z	number of teeth of the milling tool

Greek symbols

Δap	elementary axial depth of cut (height of disc)
Δt	incremental time
τ	time of passing of cutting tooth
$Ø$	tool immersion angle
$Ø_{ex}(z)$	end angle of the cut for each cutting tooth of the tool at axial position z
$Ø_{st}(z)$	beginning angle of the cut for each cutting tooth of the tool at axial position
ω_f	excitation frequency of the cutting force $F_y(t)$

ABBREVIATIONS

FE	finite element
FEM	finite element method

ПРЕДВИЂАЊЕ ХРАПАВОСТИ ПОВРШИНЕ ТАНКИХ ДЕЛОВИ СА ЗИДОВИМА НА КОЈЕ УТИЧУ ВАРИЈАЦИЈЕ РАДИЈАЛНЕ ДУБИНЕ РЕЗАЊА ТОКОМ ПЕРИФЕРНОГ ПРОЦЕСА ГЛОДАЊА

А. Садредин

Током процеса периферног глодања долази до великих вибрација попречног померања танкозидног дела под дејством сила ивице алата за глодање због њихове ниске динамичке крутости и радијалних варијација дубине реза. У овом раду се процењују главни параметри храпавости површине за стабилне услове процеса глодања кроз максималне радијалне помаке утврђене теоретском методом и прорачуном коначних елемената (kE) коришћењем нумеричких симулација. Силе ивице резног зуба се израчунавају дуж ефективног дела за сваки алат за зубе укључен у материјал дела у дискретним просторним и временским корацима помоћу глодала са равним крајевима. Коначно, суочени су радијални помаци, који су блиски по величини и тренду облика профила. Стога су генерисане силе ивице резног зуба показале постепену стабилност при промени параметра ае са 05 мм на 0,75 мм, респективно. Затим, параметри R_a и R_k доприносе више овој стабилности него R_v.